Journal of Computer-Aided Molecular Design **18:** 597–614, 2004.
DOI 10.1007/s10822-004-5433-8

Interactions of peptide mimics of hyaluronic acid with the receptor for hyaluronan mediated motility (RHAMM)

Michael R. Ziebell[1,2,*] & Glenn D. Prestwich[2,3]
[1]*Department of Physiology and Biophysics, State University of New York, Stony Brook, NY 11794, USA;* [2]*Department of Medicinal Chemistry, University of Utah, Salt Lake City, UT 84112, USA;* [3]*Center for Cell Signaling, 421 Wakara Way, Suite 360, Salt Lake City, UT 84108, USA*

Received 24 February 2004; accepted in revised form 15 October 2004

Key words: automated ligand docking, hyaluronic acid (HA), molecular modeling, peptide mimics, protein structure prediction, receptor for hyaluronan mediated motility (RHAMM), receptor ligand complex

Summary

Using the hyaluronic acid (HA) binding region of the receptor for hyaluronan-mediated motility (RHAMM) as a model, a molecular perspective for peptide mimicry of the natural ligand was established by comparing the interaction sites of HA and unnatural peptide–ligands to RHAMM. This was accomplished by obtaining a series of octapeptide–ligands through screening experiments that bound to the HA binding domains of RHAMM (amino acids 517–576) and could be displaced by HA. These molecules were computationally docked onto a three-dimensional NMR based model of RHAMM. The NMR model showed that RHAMM(517–576) was a set of three helices, two of which contained the HA binding domains (HABDs) flanking a central groove. The structure was stabilized by hydrophobic interactions from four pairs of Val and Ile side chains extending into the groove. The presence of solvent exposed, positively charged side chains spaced 11 Å apart matched the spacing of negative charges on HA. Docking experiments using flexible natural and artificial ligands demonstrated that HA and peptide–mimetics preferentially bound to the second helix that contains HABD-2. Three salt bridges between HA carboxylates and Lys548, Lys553 and Lys560 and two hydrophobic interactions involving Val538 and Val559 were predicted to stabilize the RHAMM-HA complex. The high affinity peptides and HA utilized the same charged residues, with additional contacts to other basic residues. However, hydrophobic contacts do not contribute to affinity for peptide ligand-RHAMM complexes. These results offer insight into how selectivity is achieved in the binding of HA to RHAMM, and how peptide competitors may compete for binding with HA on a single hyaladherin.

Abbreviations: CVFF – combined valence force field; DYANA – dynamics algorithm for NMR applications; ECM – extracellular matrix; EDCI – 1-[3-(dimethylamino)propyl]-3-ethylcarbodiimide hydrochloride; Erk – extracellular signal regulated protein kinase; FAK – focal adhesion kinase; GAG – glycosaminoglycan; GCU – glucuronic acid; GnHCl – guanidinium hydrochloride; GPI – glycosyl phosphatidyl inositol; GST – glutathione-S transferase; HA – hyaluronic acid; HABD – hyaluronic acid binding domain; HPLC – high performance liquid chromatography; MAPK – mitogen activated protein kinase; NAG – N-acetyl glucosamine; NOESY – nuclear Overhauser enhanced spectroscopy; ppm – parts per million; RHAMM – receptor for hyaluronan mediated motility; TGF – transforming growth factor; TOCSY – total correlation spectroscopy.

*To whom correspondence should be addressed. Current address: NeoGenesis Pharmaceuticals, 840 Memorial Drive, Cambridge, MA 02139, USA. E-mail: mziebell@neogenesis.com

Introduction

The extracellular matrix (ECM) polysaccharide hyaluronic acid (HA) promotes cell motility, adhesion, and proliferation [1, 2] (Figure 1), and thus plays an important role in morphogenesis [3], metastasis [4] and wound healing (Figure 1) [5]. These functions are mediated through HA receptors termed hyaladherins, which are present both extracellularly and intracellularly. One such hyaladherin is a receptor for hyaluronan-mediated motility (RHAMM) (CD168) [6]. RHAMM has been shown to activate the cell signaling molecules pp125 (FAK) and p42/44 extracellular regulated kinase (Erk) by an HA dependent mechanism, implicating it in intracellular modulation of cell processes [7, 8]. Isoforms of RHAMM are considered prognostic indicators of metastatic potential of breast cancer, and recently as a leukemia marker [9]. Given its role in aberrant cell behavior, RHAMM is a potential target for drug development.

RHAMM is a unique hyaladherin having little primary and secondary structural similarities to other HA binding proteins, most notably to those in the link module family [10]. Based on the NMR-based structure of TSG-6 [11], the link module HA binding domain has a template structure comprising two α-helices and two triple-stranded β-sheets arranged around a large hydrophobic core [11–13]. The charged surface which constitutes the bulk of the HA binding site utilizes nine or more residues from separate β-sheets separated by 70 amino acids in the primary sequence [14]. This is in contrast to RHAMM, where mutation studies have identified two 11-amino acid stretches near the C-terminus separated by 15 amino acids that are required for full HA binding [15]. These regions have clusters of basic residues and have a BX_7B motif, where B is a basic residue and X is any residue except acidic, and often include a hydrophobic residue. The BX_7B motif is not, however, a reliable signature for HA binding since many proteins possess this feature [16].

Two features are common to both RHAMM and the link module family [16]. First, there is the preponderance of positively charged side chains in regions that interact with HA, indicating likely charge–charge interactions that can stabilize the complex. Second, non-polar residues are invariably present and may provide an environment that excludes water in the process of binding HA. Aromatic residues may generate Π-interactions with sugar residues and Tyr residues may form hydrogen bonds with the ligand [13].

Receptor-selective competitive antagonists for the binding of HA to RHAMM have the potential to disrupt HA–RHAMM binding, thereby abrogating a key interaction in metastasis. Both natural and artificial peptides were examined as potential ligands, since they could be selected for having a higher affinity and selectivity for RHAMM relative to other HA-binding proteins such as CD44 and link module. Peptides that bound to the HA binding domain of RHAMM might utilize the same charged side chains thought to be important for HA binding. Using an octapeptide bead library with alternating positions limited to Asp and Glu residues [17], a number of high affinity peptides were identified [17]. The affinity and sensitivity to carbohydrate inhibition in RHAMM binding of four synthetic peptides were further characterized.

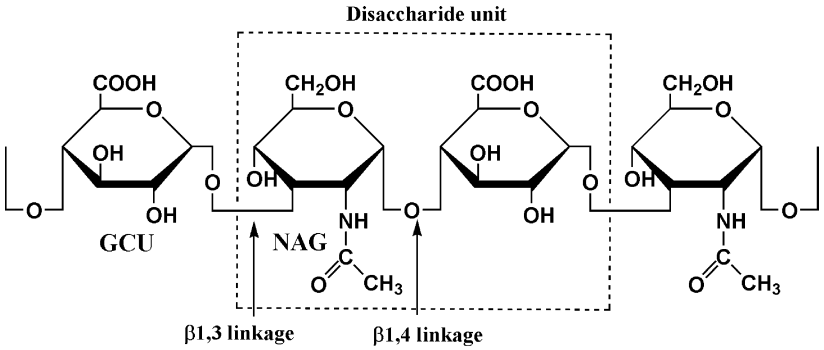

Figure 1. The chemical structure of hyaluronic acid; alternating units of glucuronic acid (GCU) and N-acetyl glucosamine (NAG). HA coil and tertiary structure are stabilized by a network of hydrogen bonds which includes one between the COOH of GCU and NH of NAG.

Table 1. Affinities of peptide ligands used in this study for RHAMM(517–576).

Name	Sequence	K_d (nM)
HA	$[GCU\text{-}NAG]_n$	100
B1	MDYEPEQE	ND
B1A	MdYEPeQe	49 (+/−3)
B1B	MDYePEQe	73 (+/−5)
B2	YDSEYESE	ND
B2A	YDSeYeSe	8 (+/−1)
B2B	YDSEYeSE	74 (+/−8)
B3	FDFDSEYE	ND
B3A	FDFdSEYe	730 (+/−25)
B3B	FdFdSEYE	1400 (+/−200)
B4	EDAENDEE	ND
B4A	EDAeNdEe	110 (+/−13)
B4B	EdAENdEe	499 (+/−75)

An eight amino acid peptide-bead library was synthesized in which alternating residues were constrained to be one of four residues: D-Asp, L-Asp, D-Glu or L-Glu. The other four positions could be any of 18 amino acids (no Pro or Cys) and all L isomers. Uppercase letters denote L amino acids and lowercase letters denote D amino acids. The affinities were determined using a solid phase binding assay in which biotinylated peptides or biotinylated HA were applied to immobilized GST-RHAMM(517–576) in a polystyrene 96 well plate and extensively washed. At increasing concentrations, a colorimetric assay determined the degree of ligand bound [17].

Table 1 summarizes the sequences and affinity of the octapeptides obtained from this study.

In order to identify specific sites of interaction on RHAMM, we combined the results of *in silico* docking calculations with a solution phase NMR model. Of particular interest was the comparison of diastereomeric pairs of peptides in which affinity was dramatically affected by a change in side chain orientation. A structural model of the HA binding domain of RHAMM was constructed using a combination of solution-phase NMR restraints and molecular modeling. Onto this template, *in silico* docking of the high affinity natural ligand (HA) and the peptide ligands was analyzed.

Methods

Sub-cloning of RHAMM(517–576) into PGEX-2T

The mouse RHAMM variant 4 cDNA in a pCRII vector [18] (Accession # CAA45848) was used as a template for PCR production of the RHAMM constructs. Sequence specific primers encoded restriction sites to permit ligation of PCR products into the appropriate vectors. Thus, the RHAMM(517–576) PCR product was digested, purified, and ligated directly into PGEX-2T (Pharmacia) using *Eco*R1 and *Bam*H1 unique restriction sites. Initial ligation of PCR products into a PGEM-T vector (Novagen) improved the ligation efficiency. Plasmid and PCR insert purification followed standard protocols, and DNA was purified by either phenol chloroform extraction or with Qiagen columns [19].

Purification of GST-RHAMM(517–576)

RHAMM(517–576) (*GS*IRDSYAQLLGHQNL KQKIKHVVKLKDENSQLKSEVSKLRSQLV KRKQNELRLQGELDKAL*GIRIHRD*) [20] was expressed in BL-21 *E. coli* cells in ampicillin-containing lubria broth by induction with IPTG (2 mM). The underlined regions denote the HABDs, and the italicized portions of the sequence are unrelated residues present as part of the expression system. Cells were harvested by centrifugation at 2000 × *g* for 30 min, resuspended in 50 PBS with 30 μg/mL leupeptin and 1 mM PMSF, and lysed using a French press at 20,000 psi. TX-100 (1% final concentration) was added to the lysate, incubated on ice for 30 min, and centrifuged at 12,000 × *g* for 30 min. The brown supernatant was applied to a 10 mL bed volume of glutathione Sepharose equilibrated in PBS at 4 °C. The supernatant was passed through the resin by gravity, the column was washed with 15–20 bed volumes of PBS at 1 mL/min, and the GST-RHAMM(517–576) was eluted with 50 mM glutathione, 10 mM Tris, pH 8.0. Fractions were collected in 50 mL falcon tubes. Each tube contained 30 mL of GST-RHAMM(517–576), the early fractions containing the most concentrated material. Only the first three fractions were cleaved with thrombin, while the remaining protein was saved for screening and binding assays. The yield of purified GST-RHAMM(517–576) was 50 mg/L in LB and 20 mg/L in minimal media. Thrombin was added to each tube at a concentration of 1 unit per mg of fusion protein. The tubes were incubated at 37 °C for 1 h. With a concentration greater than 5 mg/mL, a white precipitate was formed during the incubation time. This material, which was determined to be a 6.5 kD peptide by SDS-PAGE, was collected by centrifugation at 60,000 × *g* for

50 min. For NMR experiments, the precipitate was redissolved in 6 M GnHCl and fractionated using C8 semi-preparative HPLC, running a gradient of 20–60% acetonitrile monitoring absorbance at 254 nm. Two absorbance peaks were observed, one eluting at ~30–33% acetonitrile and another larger peak eluting at ~52–56% acetonitrile. Mass spectrometry identified the first peak as RHAMM(517–576) and estimated from SDS PAGE to be 90–95% pure. Peak fractions containing RHAMM(517–576) were collected, pooled in 10 mL glass tubes, and frozen on dry ice. Aliquots were lyophilized, and the resulting dry peptide was stored at −30 °C until use.

Minimal media expression of RHAMM(517–576) for ^{15}N labeled protein

The pGEX-2T-RHAMM(517–576) plasmid was transformed into competent BL-21-DE3 cells. An aliquot (10 mL) of an overnight lubria broth starter culture was used to inoculate 6 L of complete M9 minimal media with 5 g/L multi vitamins (Central-Vite, Western Family Foods, Portland, OR) with no isotopic label present [21]. This culture was grown to OD_{600} 0.7, and the cells were pelleted by centrifugation in 500 mL bottles at $3500 \times g$ for 30 min. The cell pellets were then resuspended in 2 L of ^{15}N labeled M9 minimal media (Martek, Columbia, MD) and grown for an additional hour, followed by induction with IPTG (2 mM) for 5 h. During induction, the pH of the culture was maintained at 7.2 with 1 N NaOH. The cells were harvested as above and the protein was purified.

Sample preparation for nuclear magnetic resonance experiments

For both unlabeled and isotope enriched experiments RHAMM(517–576) was expressed and purified as above. The final step of purification utilized semi-preparative HPLC followed by lyophilization. The two buffers used in NMR experiments were 50 mM sodium phosphate monobasic (NaH_2PO_4), pH 5.5, 0.1 mM EDTA, 10% D_2O (Cambridge Isotopes) and 130 mM potassium phosphate dibasic (K_2HPO_4), pH 8.5 unadjusted, 0.1 mM EDTA, 10% D_2O. The buffers were filtered and degassed prior to dissolving peptide in them. The peptide immediately dissolves into solution if the concentration does not exceed 2 mM. The aggregation state of the protein was observed using NMR. At high concentrations >1.5 mM, line widths indicated poorly dispersed molecules in solution. while at lower concentrations the peptide was stable in solution for one month in NMR buffer at pH 5.5. For experiments in 100% D_2O, K_2HPO_4 was dissolved in D_2O to promote exchange of protons in the salts, and then lyophilized. The lyophilized salts were then reconstituted in D_2O to 130 mM, and then the peptide was dissolved in this buffer. The peptide sample concentration was calculated by measuring the absorbance at 280 nm in a 1 mm cuvette. Shigemi tubes (5 mm, Shigemi Corp.) tuned to D_2O were used in all experiments with a total volume of 250 μL of 1–2 mM peptide.

NMR data collection and processing

NMR data on RHAMM(517–576) was collected on a Varian Inova 600 MHz spectrometer or a Varian Unity 500 MHz NMR spectrometer. ^{15}N HSQC-NOESY and ^{15}N HSQC-TOCSY experiments used an IDTG600-5 indirect triple resonance probe and 2D HSQC data collected on the 500 MHz spectrometer used the equivalent IDTXG500-5 indirect triple resonance probe. Both 2D and 3D data sets were collected as complex in States format. The order of dimension increments in the 3D experiments was d3 followed by d2. Experiments were performed at 20 °C.

The dimensions of a typical ^{15}N-HSQC data set are 2048 points and 512 increments with 16 transients. Sweep width was 6000 Hz in the ^{1}H dimension and 1800 Hz in the ^{15}N dimension. The HSQC required phasing only in the first dimension. NOESY and TOCSY experiments normally had dimensions of 4096 points by 1024 increments with 16 or 32 transients. The sweep width was set at 6000 Hz in both dimensions.

Three 3D experiments were used in the assignments of all inter- and intra-residue peaks: one 50 ms TOCSY-HSQC, one 100 ms NOESY-HSQC and one 200 ms NOESY-HSQC [21]. The dimensions of the TOCSY-HSQC were 1024 in D1 (direct ^{1}H), 256 points in D2 (indirect ^{1}H) and 128 points in D3 (^{15}N). Sweep widths were 6000 Hz in the ^{1}H dimensions and 1800 Hz in the ^{15}N dimension, and the phasing array was phase 2, phase. The 100 ms NOESY-HSQC experiment

had dimensions of 1024 points in D1 (direct ^{1}H), 128 points in D2 (^{15}N), and 256 points in D3 (indirect ^{1}H). The sweep widths were 6600 Hz in the ^{1}H dimensions and 1800 Hz in the ^{15}N dimension. For the third dimension the order of phasing was phase, phase 2. The third data set used for sequential assignments was a NOESY-HSQC with 200 ms mixing time. The dimensions were 2048 points in D1 (direct ^{1}H), 64 points in D2 (^{15}N), and 512 points in D3 (indirect ^{1}H). The sweep widths were 6000 Hz in the ^{1}H dimensions and 1800 Hz in the ^{15}N dimension. This data set provided the most information, partly because the sample was very clean and the data set had few imperfections in it and also because 200 ms mixing time allowed for magnetization transfer to extend well into the side chains.

Data processing was accomplished on a Silicon Graphics Octane using IRIX 6.5. The amide region of the ^{15}N-edited spectra was transformed from 4.7 to 10 ppm. The solvent suppression protocol used was time domain convolution with a sinebell convolution function with width 12 Hz extrapolated linearly. The window function in all dimensions was generally a sinebell with a 90° phase shift utilizing all the points in the given dimension. Baseline correction was usually not necessary. The data were transformed using Fast Fourier Transforms, and phasing was interactive. Linear prediction in the D2 (t2) dimension was not seen to improve the quality of the spectrum. The data were inspected for validity and quality in Felix97 (Molecular Simulations Inc.) and were then imported into XEASY (ETH Automated Spectroscopy for X Window Systems, Institute of Molecular Biology and Biophysics, ETH-Hönggerberg, Zürich, Switzerland) [22]. The peaks were picked in XEASY by the manual peak picking command. The amide diagonal peaks for all apparent spin systems were numbered. This gives the strip mode a peak from which to form spin system strips. Strips that represent each amino acid spin system were chosen using the strip sequence command. These strips were the basis for generating sequential assignments. All sequential assignments were completed by manually inspecting the strips and making decisions based on apparent connectivities in the N–N (amide to amide), N–α (amide to alpha), and N–β (amide to beta) regions. The TOCSY-HSQC data showed which peaks belonged to a given spin system, while the NOESY showed this information and through space connectivities within and between spin systems [23]. In addition, knowledge that the peptide is mostly helical allowed one to search for i–i + 2 N–N peaks and i–i + 2, i–i + 3, and i–i + 4 connectivities in the alpha region. Once sequential assignments were completed and verified to be consistent, all side chain peaks were labeled in the 3D NOESY spectra using the TOCSY information. Constraints for minimization were obtained by assigning all inter- and intra-residue through space connectivities [24, 25].

DYANA structure calculations

The integrated and assigned peaks were input into DYANA [26]. Angular constraints were generated using the module HABAS, which computes distance constraints to generate allowable angles in 3D space. These were then recorded as angular constraints. One hundred structures were calculated with 32,000 annealing steps. The program created 20 pdb files of the lowest energy structures.

Threading of RHAMM tertiary structure

To further refine our NMR structure of the HABD we used a series of threading algorithms that begin from the primary sequence and use proteins of known tertiary structure to predict the structure of RHAMM. We used the 3D-PSSM fold prediction threading algorithm [http://www.sbg.bio.ic.ac.uk/~3dpssm/] and the UCLA/DOE fold Server [http://fold.doe-mbi.ucla.edu/] [27, 28]. Briefly, folds are assigned using the SDP method. This computes the compatibility of the query sequence to each member of a database of three-dimensional folds by matching residue type and observed secondary structure of proteins with known three-dimensional structures to properties predicted from a query sequence. We threaded both the full length of RHAMMv4 and the subset of 62 amino acids in RHAMM(517–576).

Ligand docking onto the HABD of RHAMM

The DOCK suite of programs was used to identify favorable orientations of ligands in the receptor [29, 30]. Briefly, a subset of the protein is identified as the domain(s) of interest about which a set of predefined spheres are generated. The spheres

provide the steric and energetic restraints that dictate optimal binding of the ligand. To orient a ligand within the active site, some of the sphere centers were 'matched' with ligand atoms. An energy scoring function based on van der Waals and Coulombic forces is used to evaluate each docked position that then is provided to the user. Ligand atoms were matched with sphere centers, and distances were compared at each iteration. HA used in docking was taken from the crystal structure of a tetrasaccharide of HA (Ascension 4HYA). Peptide–ligands were considered to be β-sheet at the outset and submitted to minimization and dynamics prior to docking. In most cases this generated an extended peptide conformation. Energy grids were generated using the GRID module with a 0.2 Å grid and 4r distance-dependent dielectric [31]. The contact cutoff distance was set to 4.5 Å, the energy cutoff distance was set at 8 and the Leonard–Jones Potential equation coefficients were set to 6 for the attractive exponent and 12 for the repulsive exponent. The bump overlap was set to 0.75. A full list of parameters used in DOCK is reported in the Supplementary Material, Table S1.

A Connolly surface was generated of each atom of RHAMM(517–576) using the program MS (Biohedron) [32, 33]. The output from MS was used in the generation of sphere centers by the program SPHGEN [34], which describes the molecular surface. For the formation of spheres we set dotlim, the limit of how close two large spheres can be to one another, to 0.4. The maximum radius of spheres was set to 4.0 Å, and the minimum sphere radius was set to 1.4 Å. Initial sphere sets generated by SPHGEN were reduced in number by manually deleting extraneous spheres using InsightII (Molecular Simulations Inc.) to yield sets of 300 well-dispersed spheres covering residues 530–560. Once the data from GRID and SPHGEN were compiled, flexible docking experiments were performed with DOCK using energy (Amber force field), contact and chemical scoring [35, 36]. For comparative purposes, only the energy scoring value was used.

Both natural and unnatural peptides were considered to be β-sheet at the start of the docking procedure. The output from DOCK was imported into InsightII along with RHAMM(517–576). All docked complexes were subjected to molecular dynamics and minimization using the Discover module within InsightII using the Consistent Valence ForceField. The assemblies were soaked in a solvent shell using the layer method ensuring that the minimum solvation shell thickness around RHAMM(517–576) was 4 Å. The solvated assemblies were subjected to 1000 steps of molecular dynamics at 313 K and constant pressure, followed by 500 minimization steps using the steepest descent method with charges and cross terms. These sets of molecules were evaluated for overall consistency and steric constraints. The final images for publication were prepared in pymol (http://www.pymol.org).

Results

Structure of the HA binding domain of RHAMM

An NMR-based model of the HA binding domain of RHAMM was constructed in order to examine the mechanism of HA binding and the regulatory role ligand binding might play in conformational changes of RHAMM. Circular dichroism experiments showed that RHAMM(517–576) was predominantly helical, and that this native helical structure was recovered after HPLC purification followed by lyophilization and resolubilization in NMR buffer (50 mM NaH_2PO_4, pH 5.5, 0.1 mM EDTA, 10% D_2O). The purified peptide also had full HA binding activity based on evaluation of binding using a dot blot assay. A pH dependent structural shift in RHAMM(517–576) occurred, such that the molecule was maximally helical at pH 7.2 (Figure 2). In order to retain signal from exchangeable amide protons, resolution was sacrificed in order to visualize the structural elements at the site of HA binding in RHAMM.

The sequence of RHAMM(517–576) includes 11 leucines and collectively 13 lysines and arginines with no prolines or disulfides. Because of the lack of amino acid diversity and because the secondary structure is helical, the ^{15}N-HSQC peaks span only 1.2 ppm excluding aromatic side chains (Figure 3). Backbone spin system identification was accomplished using ^{15}N-HSQC-TOCSY and sequential assignments were completed using 200 ms ^{15}N-HSQC-NOESY. One hundred nine short range NOEs and seven long range NOEs were found with two short range NOE violations. Stereospecific assignments were possible in 20 out of 90

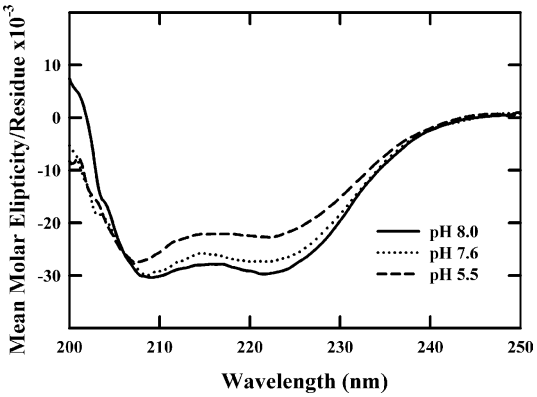

Figure 2. Circular dichroism of RHAMM(517–576) with 30 mM potassium phosphate pH 5.5, pH 7.6 and pH 8 at 5 °C. Data collected on a JASCO from 200 to 250 nm at 0.05 nm/point, 0.5 s/point and 50 mdeg/FS and smoothed after collection.

possible stereoselective locations on the peptide. The final minimized structure of RHAMM(517–576) had an RMSD of 4.2 Å. RHAMM(517–576) was used as the primary structure template in a series of threading experiments. The highest scorer was 78 amino acid NK Lysine (PDB accession ID 1NKL) with a Z score of 2.26.

From the NMR results enhanced by threading, the structure was found to consist of three helices numbered from the amino terminus: HX-1 (Arg518-Lys539), HX-2 (Ser545-Lys562) and HX-3 (Glu565-Lys574) with two loops, L-1 (Leu540-Asn544) and L-2 (Gln563-Asn564) (Figures 4 and 5). HX-1 and HX-2 flank a central groove with the first BX_7B motif HABD-1 (Lys531-Lys541) completely contained within HX-1, while the second HABD-2 (Lys553-Lys562) spans HX-2 and a portion of L-2 (Figure 5). Eleven aliphatic residues create a hydrophobic core in the pocket created by the three helices, which acts to stabilize the tertiary structure. Four pairs of aliphatic side chains extend into the cavity excluding water while all basic residue side chains of HX-1 and HX-2 extend away from the hydrophobic cleft. NOE distance constraints from three of these pairs that assisted in establishing the relationships between helices are represented in Figure 4: Val538 to Val551, Leu554 to Leu530 and finally Leu576 to Ile534. The inset demonstrates the spatial relationship between these aliphatic residues that renders them essential to creating the hydrophobic core that stabilizes the three helices. Three hydrogen bonds at opposite ends of the helices help maintain the spatial relationship between the helices: between HX-1 and HX-2 there is a hydrogen bond between Gln523 and Lys553 and between HX-1 and HX-3 there is one hydrogen bond between Gln532 and Asp573. The loop structures are maintained each by a hydrogen bond, between Asp543 and Lys548 for L-1 and one between Lys560 and Gln563 for L-2. Two aliphatic residues (Leu520 and Leu521) are solvent exposed at the beginning of HX-1. The amino and carboxy termini that include non-RHAMM sequence maintain unstructured segments spanning four and six residues, respectively.

Docking of ligands onto RHAMM(517–576)

Tetrasaccharide HA, HA_{12}, and peptide–ligands were computationally docked onto RHAMM(517–576) using the same docking parameters. The peptide–ligands docked include eight amino acid peptides that comprise D acidic amino acids discovered from multiple screens (B1-A, B1-B, B2-A, B2-B, B3-A, B3-B, B4-A, B4-B), for which affinities were previously determined, as well as the all L peptides (B1, B2, B3 and B4), for which affinities were not calculated (Table 1). The ligands were docked onto RHAMM(517–576) by positioning the ligand 20 nm away from RHAMM(517–576) and initiating a DOCK search of 1000 possible orientations [27]. This was repeated 10 times under the same conditions for each ligand using different random seed number. The final docked complexes were subjected to molecular dynamics with a solvation shell followed by a final minimization and the orientation of the ligand with respect to RHAMM(517–576) was inspected to catalog the position of non-covalent interactions between the receptor and ligands.

Docking of HA onto RHAMM(517–576)

For both long and short oligomers of HA, the docked ligands consistently bound to RHAMM(517–576) utilizing the positively charged surface on HX-2 (Figures 6 and 8). HA_{12} extended across L-1, and uncoiled within the three disaccharides flanking HX-2, permitting a loop to form that positioned three glucuronate (GCU) carboxylates within 4.1 Å of three basic residue side chains of RHAMM. By virtue of the prox-

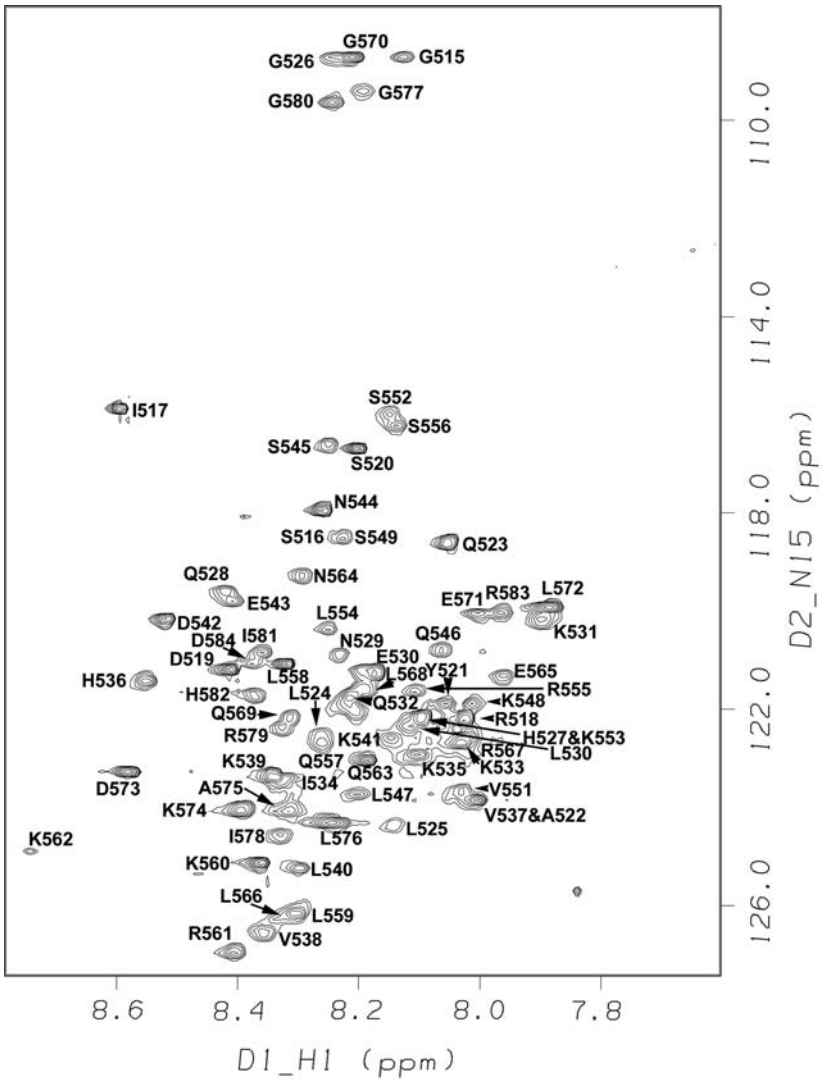

Figure 3. Backbone amide region from a 2D slice of a ^{15}N-HSQC-TOCSY experiment of RHAMM(517–576) at pH 5.5 showing the amino acid spin systems for 62 residues.

imity and orientation of the receptor's side chains with respect to the carboxylates on their partner GCU moiety on HA, these are proposed locations of salt bridges in the docked complex. Numbering from the GCU end of HA, these lie between GCU_9 and Lys548 (2.9 Å) preceding HABD-2, GCU_5 and Lys553 (4.1 Å), and between GCU_1 and Lys560 (2.9 Å), the latter two interactions falling within HABD-2. The sugar ring CH_2 groups on NAG_{10} were in close proximity to Val538 and the sugar ring CH_2 groups on NAG_2 were close to Val559, which for both of these regions suggests the exclusion of water, generating entropically favorable conditions for HA to remain bound. The resulting effect on HA is evident in the modulation of glycosidic dihedral angles recorded in Table 2 where β(1–3) and β(1–4) φ and ψ angles between GCU_1 and GCU_3 and between GCU_7 to GCU_{10} were constrained to permit interactions between Lys553 and GCU_5 and Lys560 and GCU_1.

Docking of peptide ligands onto RHAMM (517–576)

All peptides docked to a groove on RHAMM(517–576) formed by HX-2 and HX-3, with a locus of interaction centered on a pocket created by Lys553, Val559 and Arg567. The ori-

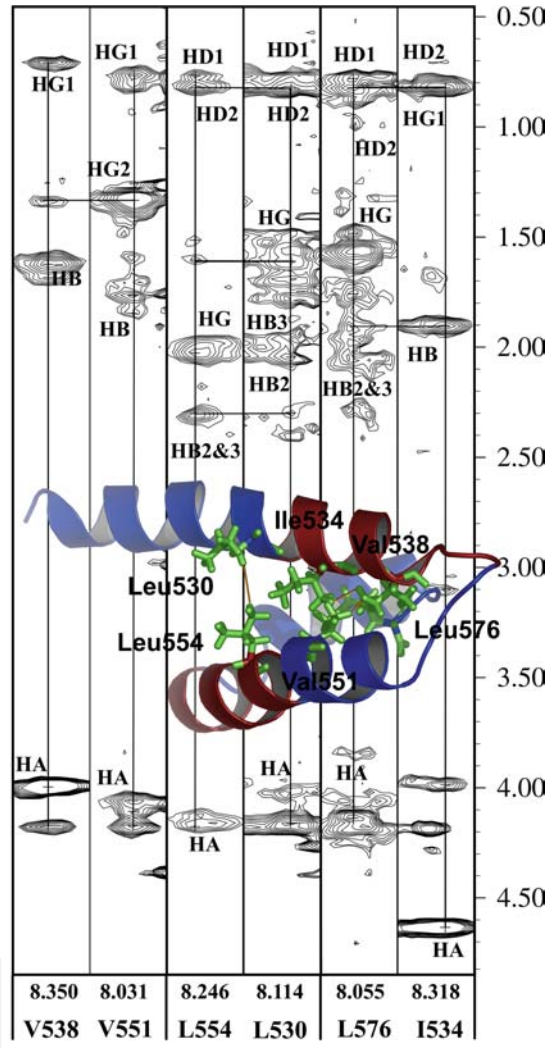

Figure 4. Three pairs of XEASY strips from an ^{15}N-HSQC-TOCSY of RHAMM(517–576) at pH 5.5 (Val538 and Val551, 2.44 Å; Leu554 and Leu530, 4.67 Å; Leu576 and Iso534, 2.15 Å); noted is the shortest distance between sidechains. These data demonstrate through-space connectivities between side chains atoms of residues thought to stabilize the hydrophobic core between helices 1 and 2. Inset: model of RHAMM(517–576) with residues corresponding to NMR strip data highlighted in green. Orange lines indicate distance restraints obtained from data.

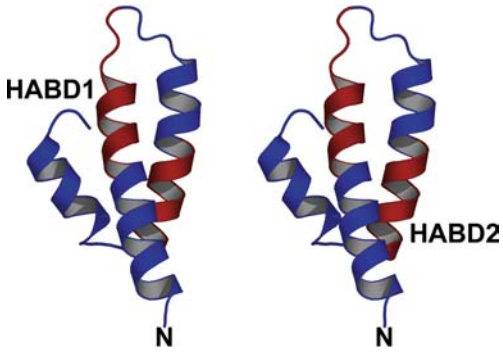

Figure 5. Stereo representation of the structure of RHAMM(517–576) based on NMR data combined with threading. Numbering of the three helices, HX-1, HX-2 and HX-3, and two linker regions, L-1 and L-2 is relative to the N-terminus. HABD-1 (RHAMM(531–541)) extends from within HX-1 into L-1 while HABD-2 (RHAMM(553–562)) is contained within HX-2.

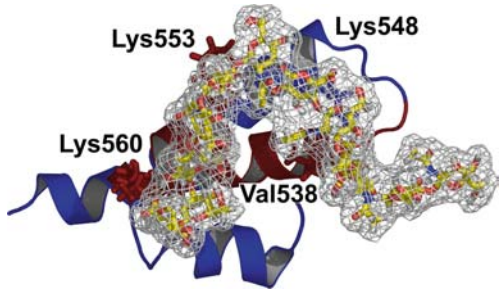

Figure 6. Dodecasaccharide HA docked as a flexible ligand onto RHAMM(517–576) using DOCK 4.0 viewed from the 'bottom' side of RHAMM(517–576). Residues on RHAMM predicted to be involved in binding HA are rendered colored red if in HABD1 or HABD2 and blue if not in either. At least three salt bridges are predicted to stabilize the HA-RHAMM complex: Lys548 to GCU9 (2.9 Å), Lys553 to GCU5 (4.1 Å), and Lys 560 to GCU1 (2.9 Å). The latter two lysines are in HABD2. Two possible hydrophobic interactions are considered between Val538 and the CH_2 face that includes NAG10 (2.5 Å) and Val559 (hidden, see Figure 8) and the CH_2 face of NAG2 (2.4 Å) (Table 2).

entation of the peptides falls into two general groups: those ligands that bind parallel to HX-2 and those that bind more or less orthogonal to HX-2 (Table 3, Figure 7 and Supplementary Figures 1–4). Three of the ligands that lie parallel to HX-2—B-1, B2-A, B3-A and B4, extend side-chains into the space created by HX-2 and HX-3. These are designated 'PI' in Table 3. B2-A, B3-B and B4-B lie external to the HX-2/HX-3 cavity, flanking HX-2 forming salt bridges with positive charges and are designated 'PE' in Table 3. Of the ligands that lie orthogonal to HX-2, B1-A and B2 contact the HX-2/HX-3 cavity and are designated 'OI'. Four ligands (B1-B, B2-B, B3 and B4-A) fail to interact with this space because their favored docking orientation extends side chains away from the cavity. These are designated 'OE' in Table 3.

A catalog of the sites of interaction between RHAMM(517–576) and peptide–ligands was gen-

Table 2. Dihedral angles for undocked and docked HA.

	Undocked HA		Docked HA	
	φ	ψ	φ	ψ
NAG_{12}-GCU_{11} β(1-4)	−16.4	37.5	−27.2	−21.4
GCU_{11}-NAG_{10} β (1-3)	21.8	54.4	154.3	44.4
NAG_{10}-GCU_{9} β (1-4)	−16.3	37.3	42.4	109.1
GCU_{9}-NAG_{8} β (1-3)	21.7	54.4	87.8	−131.6
NAG_{8}-GCU_{7} β (1-4)	−16.3	37.3	46.1	119.4
GCU_{7}-NAG_{6} β (1-3)	21.0	53.6	16.1	44.4
NAG_{6}-GCU_{5} β (1-4)	−16.4	37.4	−45.0	−56.2
GCU_{5}-NAG_{4} β (1-3)	21.8	54.4	167.6	19.1
NAG_{4}-GCU_{3} β (1-4)	−16.4	37.3	52.9	34.5
GCU_{3}-NAG_{2} β (1-3)	21.8	54.4	178.7	−163.5
NAG_{2}-GCU_{1} β (1-4)	−16.3	37.3	164.7	177.5

The definitions used for φ and ψ angles were NAG(H1)-NAG(C1)-GCU(O4)-GCU(C4) and NAG(C1)-GCU(O4)-GCU(C4)-GCU(H4), respectively for the β(1-4) glycosidic linkage and GCU(H1)-GCU(C1)-NAG(O3)-NAG(C3) and GCU(C1)-NAG(O3)-NAG(C3)-NAG(H3) for the β(1-3) glycosidic linkage. Undocked values were taken from the protein data bank (http://www.rcsb.org), accession number 4HYA.

erated, and subdivided into contacts that contributed either positively or negatively to the energetics of the interaction (Table 3). Positive contributions consisted of electrostatic attraction and hydrophobic interactions while negative contributions were defined as same charge side chains within a radius of 4 Å. Eleven out of 12 peptide ligands contained an acidic side chain within a 4 Å radius of Arg555 sufficient to favor the formation of a salt bridge, but the same position is not employed in each series. For example, B2-A D-Glu4 and B2-B L-Asp2 are in close proximity to Arg555 and B4-A D-Glu4 and B4 D-Asp6 are also near Arg555. Furthermore, this residue does not appear to interact directly with HA. The next most important RHAMM residue for ligand interactions is Lys560, which was predicted to interact with half of the peptide ligands and also with HA followed by Lys553. These three basic residues that form the locus of interaction between ligands and RHAMM all are within HABD-2. Three ligands had side chains in close proximity to RHAMM amino acids in HABD-1—B1 and B4-A with Lys531 and B2 with Lys539. The rest interacted with basic and aliphatic residues N-terminal to and within HABD-2. Hydrophobic contacts between RHAMM(517–576) and peptide–ligands were possible between a subset of ligands, B2 and B3-A, both of which are thought to have low affinity for RHAMM(517–576). In contrast, HA has two possible contacts with hydrophobic residues and this is proposed here and in other work to contribute towards affinity between HA and RHAMM [13]. Finally the proximity of acidic residues on B2 and B4 and Glu571 are thought to negatively affect affinity.

Discussion

The three-dimensional structure of RHAMM(517–576) differs substantially from other known structures of HA binding proteins in which β sheets dominate the HA binding domain [11, 14, 37]. Instead, the two predicted HABDs of RHAMM are contained within separate highly basic coiled regions that flank one another about a central groove. All but 2 of the 15 aliphatic side chains from HX-1 to HX-3 extend inward to form a hydrophobic interior (Figure 4), which we propose serves to stabilize the secondary structure. That HX-1, HX-2 and HX-3 appear tightly bundled suggests they represent a distinct domain in full length RHAMM. The majority of the 13 lysine and arginine side chains are solvent exposed, creating a positively charged surface on both HX-1 and HX-2. The results from docking natural and artificial ligands presented here suggest that the majority of interactions are with the positively charged surface surrounding HX-2, the location of HABD-2, with minimal association of ligands with the hydrophobic core.

Table 3. Interactions of RHAMM(517–576) with HA and peptide ligands.

Distance (Å) Followed by Interacting Residue from Ligand (lower case = D amino acid)													
	HA	B1	B1A	B1B	B2	B2A	B2B	B3	B3A	B3B	B4	B4A	B4B
K_d	100[a]		49	73		8	74		730	1400		110	550
Orientation		PI	OI	OE	OI	PE	OE	OE	PI	PE	PI	OE	PE
Residue	Electrostatic Attractive												
Lys531		2.9 E6										2.3 e4	
Lys539					2.9 E8								
Lys548	2.9 GCU9					2.9 D2		2.4 D2			2.7 D6	2.7 D2	2.8 d6
Lys553	4.1 GCU5			2.7 E6			2.8 E8	3.03 E8					
Arg555		3.0 E6	3.1 E4	2.8 D2		2.6 e4	3.0 D2	3.0 E6	2.9 d4	1.8 E6	1.8 D6	1.8 e4	1.9 d6
Lys560	2.9 GCU1	3.0 E4	1.9 e6			2.9 e6				1.7 d4	3.2 E1	2.2 d6	
Arg567					2.6 E4								
Lys574		3.2 E8											
	Hydrophobic												
Val538	2.5 NAG10												
Val559	2.4 NAG2		2.7 P5		2.9 Y1		2.8 Y4		3.6 F3				
Leu576					2.7 Y5								
	Electrostatic Repulsive												
Glu571					4.0 E4						2.8 E8		

The first column indicates the RHAMM residue from which the distance is measured. Rows with dark grey background are residues in HABD-1 and rows with light grey background are residues in HABD-2. The values shown are distances between terminal side chain atoms on receptor and ligand in Å. The corresponding residue on the ligand to which contact is made is shown after the value with a capital letter indicating L amino acids and a lower case letter indicating D amino acids. Electrostatic interactions are defined as distances under 4.2 Å between side chains of opposite charge. These are most likely salt bridges but may also be hydrogen bonds. There were no cases of negatively charged side chains on RHAMM interacting with positively charged side chains on any ligand. Hydrophobic interactions are defined by proximity of 3.2 Å or less between aliphatic residues on RHAMM and aliphatic or hydrophobic residues on the ligands. Interactions that cause a reduction in affinity are classified as proximal residues on the ligand and RHAMM with the same charge. In these experiments there were two examples of repulsion with Glu571 in HABD-2. Orientation codes refer to ligand orientations relative to HX-1 where 'O' signifies orthogonal, 'P' signifies parallel, 'I' indicates that portions of the ligand lie internal to the cavity created by HX-1 and HX-3, while 'E' indicates that the entire ligand remains outside of this space. See text, Figure 7 and Supplemental Figures 1 to 4. [a]The affinity for HA was obtained from [42].

HA affinity determinants on RHAMM

In our model, HA binding to RHAMM requires the unraveling of HA from its native twofold helix to its highly irregular and constrained structure bound to RHAMM because the distances between basic side chains on either HABD-1 or HABD-2 do not match the 8.9 Å distance between GCU carboxylates on helical HA. The stepwise process by which this occurs is poorly understood given the complex tertiary structure of extracellular HA, but the end result is the formation of three salt bridges identified in our model formed between docked HA_{12} and RHAMM(517–576): Lys548 with GCU_9 preceding HABD-2, Lys553 with GCU_5 and Lys560 with GCU_1 (Figure 6, Table 3). Each of these would contribute ~40 kJ/mol to the free energy of binding to the receptor-ligand complex. Furthermore, in the process of unraveling, the hydrophobic interactions that are present in stacked HA antiparallel chains [38] are disrupted upon binding to RHAMM. Val538 and Val559 are sufficiently close (< 3.2 Å) to the hydrophobic face of HA to exclude water, providing an additional 10–20 kJ/mol free energy of binding.

Taken together, electrostatics are the major contributor to the stabilization of the bound

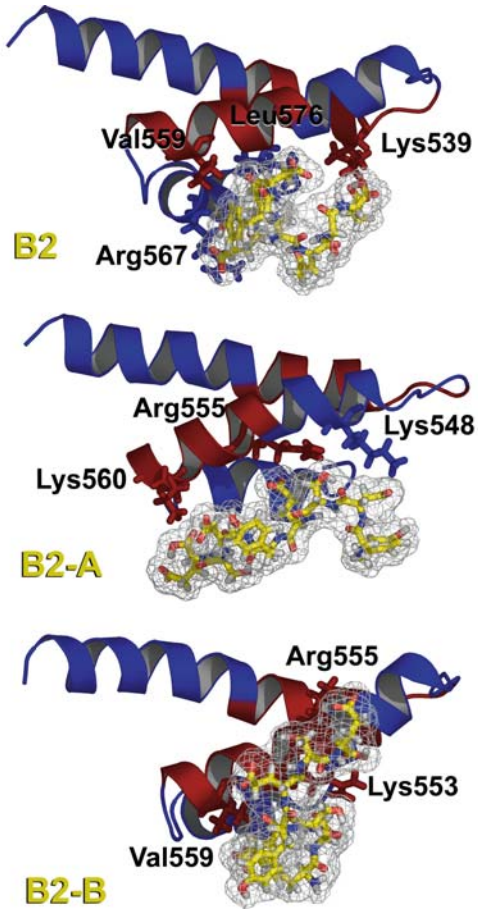

Figure 7. B2 (YDSEYESE) (top), B2-A (YDSeYeSe) ($K_d = 8$ nM, middle), and B2-B (YDSEYeSE) ($K_d = 74$ nM, lower) docked onto RHAMM(517–576). Shown are RHAMM basic residues in each complex predicted to interact with the peptide ligands. The orientation of B2 is such that it fails to form a salt bridge with Lys553, Arg555 or Lys560 as do B2A or B2B (see Table 3). B2-A, the highest affinity ligand in this series, forms three salt bridges with RHAMM residues Lys548, Arg555 and Lys560, while B2-B forms salt bridges with Lys553 and Arg555.

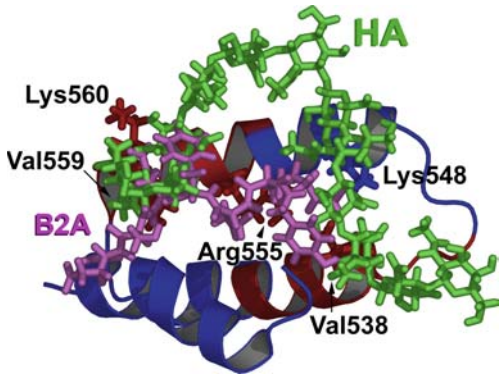

Figure 8. View of RHAMM(517–576) with the minimized conformations of both HA and B2-A docked, indicating residues common to both sets of interactions. Val538, Lys548, Lys553, Val 559 and Lys560 are involved in HA interactions with RHAMM(517–579), while Lys548, Arg555 and Lys560 are involved in B2-A interactions with RHAMM(517–579).

complex, but the two hydrophobic contacts at Val538 and Val559 provide no more than 20% of the free energy of binding for this protein–ligand interaction. This data is supported by previous studies supporting the role of hydrogen bonding and ionic interactions in protein interactions with HA [14], while other studies have pointed to protein interactions that specifically harness the hydrophobic character of HA [39–41]. Other GAGs such as heparin and chondroitin sulfate–C bind to RHAMM but with 10-fold less affinity [42]. Given the effectiveness of HA in harnessing the positively charged surface on HX-2 for binding, this difference is most likely due to inadequate utilization of these charges by other GAGs. Recently, Cai and co-workers designed a high-affinity, HA-selective binding protein by linking three repeats of the RHAMM HABD in tandem. The resulting construct exhibited a loss of high-affinity HA binding and a 100-fold increase in its affinity for heparin. Importantly, an experimental analysis based on polyelectrolyte theory documented that the contribution of purely electrostatic interactions to this affinity was only 28%, confirming a 72% structural basis for the high affinity [43]. This demonstrates that for heparin, increased charge density alone can account for increased affinity, while for HA, affinity is more sensitive to protein structure. This may be a reflection of the need for appropriate spatial relationships betweeen aliphatic and charged amino acids in RHAMM that is present for HA but not for other glycosaminoglycans.

HA_{12} bound to RHAMM(517–576) unraveled sufficiently to permit a bend between GCU_3 and GCU_5 not observed in solution structures of HA (Figure 6 and Table 2). This conformation was generated by smaller, allowable glycosidic φ,ψ angles between saccharides. The resulting compact HA strand then maximizes binding affinity by interacting with Lys548, Lys553 and Lys560 on the HA binding surface of RHAMM. This is in contrast to the conformation of HA_8 in the

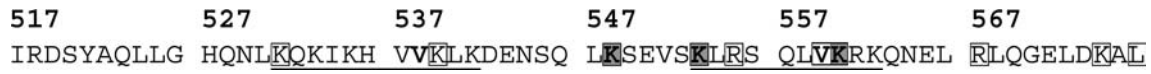

Figure 9. Summary of residues implicated in ligand binding to RHAMM(517–576). Bolded letters indicate predicted interactions with HA while boxed letters indicate interactions with peptide–ligands. Underlined regions show the locations of HABD-1 and HABD-2. Grey boxed positions indicate residues that contribute to a high affinity interaction with either HA or peptide–ligands.

TSG-6 binding groove that, from a simple docking model, optimally occupies the HA binding groove by gradually bending around the link module [14]. In this model for HA_8, TSG-6 residues Lys11 and Arg81 form salt bridges with GCU sugars and aromatic residues Tyr59, Phe70 and Tyr78 involved in ring stacking with the hydrophobic face of HA. Tyr12, Tyr59 and Tyr78 are also thought to form hydrogen bonds with HA. This greater dependence on hydrophobic residues to stabilize HA binding is not observed in RHAMM [37]. With only one tyrosine in RHAMM(517–576) and no other aromatic residues, HA binding in RHAMM must be mediated by the spatial distribution of positively charged residues and possibly an aliphatic residue. It appears from this analysis, therefore, that fundamental differences in modes of HA binding exist among HA binding proteins, which is reflected in the gross differences in tertiary structure between TSG-6 and RHAMM.

Affinity determinants of library hits compared to HA

Similar to the RHAMM-HA complex, electrostatic interactions increase peptide–ligand affinity to the RHAMM-HABDs. Peptide affinity can be correlated to the number of salt bridges it is predicted to form in the complex (Table 3). The highest affinity peptide (B2-A) has three contact points while peptides from the weakest (B3) series have either one or two. Furthermore, all high affinity interactions with either HA or peptide ligands necessarily include at least two interactions with the core basic residues Lys548, Lys553 and Lys560, all of which are utilized by HA. Lys553 is central to most peptide interactions but not to HA. Lower affinity peptides fail to contact two out of these three basic residues. These data suggest that affinity depends on multiple electrostatic interactions but not one particular set of interactions provides significantly more binding energy than another. Selection of particular interactions depends on orientation of charges on the ligand as well as on steric constraints inhibiting interaction. This coincides with the observation that orientation alone is not a determinant of affinity, since the highest affinity ligand (B2-A) docked parallel to HX-2 while the second highest affinity ligand (B1-A) docked orthogonally to HX-2. One unexpected result is the similarity of interactions between B2-A and B4-A while B2-A was determined to have 10-fold higher affinity.

Unlike HA, there is no correlation between hydrophobic interactions between RHAMM and peptide–ligands, arguing that affinity in the case of peptide–ligands is driven by electrostatics alone. Nonetheless, the selection of aliphatic and aromatic side chains in the screening process indicates the importance of non-polar groups on the peptide–ligands to generate high affinity to RHAMM. Non-polar side chains may be involved in positioning ligand negative charges such that they interact with corresponding positive charges on RHAMM(517–576).

That all ligands favored docking space near HX-2 is surprising given the distribution of positive charge in HX-1 as well as HX-2. The preference of HA and peptide–ligands for HX-2 may be a result of a greater concentration of positive charge on HX-1 as well as morphological constraints on the HX-1 side of the domain. A densely charged region on HX-2 extends from residues 560 to 567 and includes four basic residues, two of which stabilize HA binding and all of which are encountered with various peptide–ligands. An overlay of the docked HA and docked B2-A onto RHAMM (Figure 8) demonstrates the presence of common sites of interaction. Instances of a single ligand simultaneously binding to both helices are rare because of two morphological constraints. First, the surface of RHAMM(517–576) formed by parallel HX-1 and HX-2 contains a V-shaped cleft that is formed with a hydrophobic interior (Figure 4, inset). This would require a hypotheti-

cal ligand with a unique shape to both fit into the groove and utilize charges on either side of the groove. Because the positively charged side chains extend away from the interior, a negatively charged polymer extending the length of this cleft would fail to utilize the majority of these surface charges. Second, the charged surface of RHAMM(517–576) HABD-1 most amenable to interactions with charged ligands is obstructed by HX-3. This does not exclude a role for HABD-1 in HA binding, but it suggests that HABD-1 may be more important for interactions with higher order HA oligomers.

Effects of unnatural amino acids in peptide libraries

We designed a family of polyanionic peptide–ligands to mimic HA by spacing negative charges at intervals similar to that of the natural ligand. This was achieved by alternating residues with either D or L isomers of aspartates or glutamates in which the distance between charges ranges from 8 to 14 Å depending on the dihedral angles between the three residues. The inclusion of D isomers increased the flexibility that generated a wider range of conformers within a single family. The differences in affinity are most apparent in the B2 family with a 10-fold difference between B2-A (YDSeYeSe) and B2-B (YDSEYeSE) and to a lesser extent B1-A (MdYEPeQe) vs. B1-B (MDYePEQe), and B4-A (EDAeNdEe) vs. B4-B (EdAENdEe) (Table 1). The A and B peptides from each of these families represent the highest affinity of 16 possible diastereomers that were analyzed for their ability to bind competitively to RHAMM(517–576).

The opposing isomers of the B2 family generate strikingly different conformations of the docked peptides (Figure 7) in which B2 and B2-A are oriented parallel to HX-2 and HX-3 while B2-B with lower affinity lies orthogonal to the helices. A consequence of this is the formation of different numbers of salt bridges for these docked complexes: B2 has two contacts, B2-A ($K_d = 8$ nM) has three contacts, and B2-B ($K_d = 74$ nM) has two contacts. Both B2-A and B2-B make salt bridges with Lys553 while B2 has sufficiently different steric constraints as to prevent that interaction (Table 3). Given the flexibility of peptides, the difference in affinity is unlikely to be due to the distance between charges alone. Rather it is more likely that the dihedral angles in peptide–ligands that have both D and L acidic residues give rise to rotamers with extended acidic side chains in the same direction. This then will constrain interactions either in favor of close contact, as in the case of B2-A, or more distant contact for B2. For B2 with no unnatural residues the φ dihedral angle between L-Glu4 and L-Tyr 5 is −174°. For B2-A φ between D-Glu4 and L-Tyr5 is −96° and for B2-B φ between L-Glu4 and L-Tyr5 is −77°. It may be concluded that the rotational freedom afforded by including D-acidic residues permits contact with a greater number of charged groups on the receptor than an all L peptide. Docked HA has GCU carboxylates oriented with a dihedral angle between them measuring −164°, close to the measurements of acidic residue dihedrals in B2-A, but in this study Lys553 is not oriented close enough to form a salt bridge with GCU_5 (Figure 5) as it is for the peptide–ligands (see Table 2). This may explain the higher affinity observed for certain peptides compared to HA, whereby more contacts are possible for peptides because of their structural diversity.

Figure 9 summarizes the residues implicated in HA binding as well as peptide mimics of HA. The positions of Lys548 and Lys560 are common to both HA and peptide–ligands, but a separate set of lysines is involved solely in peptide binding. Nonetheless, the highest affinity docked peptides (B2-A, B4-A and B4-B) clearly occupy the space next to HX-2 used by bound HA. For this reason, we believe inhibition of HA binding by these peptides is not allosteric but represents blocking of binding sites by high affinity competitors. The peptides discovered in these experiments and the ensuing computational analysis of binding to RHAMM are part of a search for molecules that act as agonists or antagonists of HA binding to cell surface receptors. Additional NMR experiments of RHAMM(517–576) complexed with low molecular weight HA or with B2-A will strengthen the finding presented here. We also wish to evaluate these RHAMM-specific ligands for their ability to induce motility in fibroblasts, or to block HA from doing so.

Acknowledgements

The authors are grateful to Professor I. Kuntz for providing DOCK. Many thanks to Prof. Darrell

Davis, Dr. Tim Stemmler, and Dr. Steve Alam (Biomolecular NMR Facility, University of Utah Health Sciences Center) for useful discussions and assistance with instrumentation.

This work was supported by grants to G.D.P. from the Department of Defense, the State of Utah Centers of Excellence Program, and the University of Utah. This article must therefore be hereby marked "*advertisement*" in accordance with 18 U.S.C. Section 1734 solely to indicate this fact.

References

1. Fraser, J.R., Laurent, T.C. and Laurent, U.B., J. Intern. Med., 242 (1997) 27.
2. Lee, J.Y. and Spicer, A.P., Curr. Opin. Cell Biol., 12 (2000) 581.
3. Toole, B.P., Semin. Cell. Dev. Biol., 12 (2001) 79.
4. Entwistle, J., Hall, C.L. and Turley, E.A., J. Cell. Biochem., 61 (1996) 569.
5. Chen, W.Y. and Abatangelo, G., Wound Repair Regen., 7 (1999) 79.
6. Turley, E.A., Noble, P.W. and Bourguignon, L.Y., J. Biol. Chem., 277 (2002) 4589.
7. Lynn, B.D., Li, X., Cattini, P.A., Turley, E.A. and Nagy, J.I., J. Comp. Neurol., 439 (2001) 315.
8. Lokeshwar, V.B. and Selzer, M.G., J. Biol. Chem., 275 (2000) 27641.
9. Greiner, J., Ringhoffer, M., Taniguchi, M., Schmitt, A., Kirchner, D., Krahn, G., Heilmann, V., Gschwend, J., Bergmann, L., Dohner, H. and Schmitt, M., Exp. Hematol., 30 (2002) 1029.
10. Day, A.J., Biochem. Soc. Trans., 27 (1999) 115.
11. Kohda, D., Morton, C.J., Parkar, A.A., Hatanaka, H., Inagaki, F.M., Campbell, I.D. and Day, A.J., Cell, 86 (1996) 767.
12. Lesley, J., English, N.M., Gal, I., Mikecz, K., Day, A.J. and Hyman, R., J. Biol. Chem., 277 (2002) 26600.
13. Bajorath, J., Greenfield, B., Munro, S.B., Day, A.J. and Aruffo, A., J. Biol. Chem., 273 (1998) 338.
14. Blundell, C.D., Mahoney, D.J., Almond, A., DeAngelis, P.L., Kahmann, J.D., Teriete, P., Pickford, A.R., Campbell, I.D. and Day, A.J., J. Biol. Chem., 11 (2003) 11.
15. Yang, B., Yang, B.L., Savani, R.C. and Turley, E.A., Embo J., 13 (1994) 286.
16. Day, A.J. and Prestwich, G.D., J. Biol. Chem., 277 (2002) 4585.
17. Ziebell, M.R., Zhao, Z.G., Luo, B., Luo, Y., Turley, E.A. and Prestwich, G.D., Chem. Biol., 8 (2001) 1081.
18. Hall, C.L., Yang, B., Yang, X., Zhang, S., Turley, M., Samuel, S., Lange, L.A., Wang, C., Curpen, G.D., Savani, R.C. et al., Cell, 82 (1995) 19.
19. Sambrook, J., Fritsch, E.F. and Maniatis, T., Molecular Cloning, A Laboratory Manual., 2nd edn., Cold Spring Harbor Laboratory Press, Cold Spring Harbor, NY, 1989.
20. Wang, C., Entwistle, J., Hou, G., Li, Q. and Turley, E.A., Gene, 174 (1996) 299.
21. Nordstrand, K., Ponstingl, H., Holmgren, A. and Otting, G., Eur. Biophys. J., 24 (1996) 179.
22. Bartels, C., Xia, T.H., Billeter, M., Guntert, P. and Wüthrich, K., J. Biomol. NMR, 6 (1995) 1.
23. Clore, G.M., Omichinski, J.G., Sakaguchi, K., Zambrano, N., Sakamoto, H., Appella, E. and Gronenborn, A.M., Science, 265 (1994) 386.
24. Wüthrich, K., Billeter, M. and Braun, W., J. Mol. Biol., 180 (1984) 715.
25. Havel, T.F. and Wüthrich, K., J. Mol. Biol., 182 (1985) 281.
26. Guntert, P., Mumenthaler, C. and Wüthrich, K., J. Mol. Biol., 273 (1997) 283.
27. Kelley, L.A., MacCallum, R.M. and Sternberg, M.J., J. Mol. Biol., 299 (2000) 499.
28. Mallick, P., Goodwill, K.E., Fitz-Gibbon, S., Miller, J.H. and Eisenberg, D., Proc. Natl. Acad. Sci. USA, 97 (2000) 2450.
29. Ewing, T.J., Makino, S., Skillman, A.G. and Kuntz, I.D., J. Comput.-Aided. Mol. Des., 15 (2001) 411.
30. Ewing, T.J. and Kuntz, I.D., J. Comput. Chem., 18 (1997) 1175.
31. Wang, J., Kollman, P.A. and Kuntz, I.D., Proteins, 36 (1999) 1.
32. Connolly, M.L., J. Mol. Graphics, 4 (1986) 3.
33. Connolly, M.L., Science, 221 (1983) 709.
34. Hendrix, D.K. and Kuntz, I.D., Pac. Symp. Biocomput. (1998) 317.
35. Knegtel, R.M. and Wagener, M., Proteins, 37 (1999) 334.
36. Fradera, X., Knegtel, R.M. and Mestres, J., Proteins, 40 (2000) 623.
37. Mahoney, D.J., Blundell, C.D. and Day, A.J., J. Biol. Chem., 276 (2001) 22764.
38. Scott, J.E., Ciba Found. Symp., 143 (1989) 6.
39. Bray, B.A., J. Theor. Biol., 210 (2001) 121.
40. Li, S. and Jedrzejas, M.J., J. Biol. Chem., 276 (2001) 41407.
41. Nukui, M., Taylor, K.B., McPherson, D.T., Shigenaga, M.K. and Jedrzejas, M.J., J. Biol. Chem., 278 (2003) 3079.
42. Yang, B., Hall, C.L., Yang, B.L., Savani, R.C. and Turley, E.A., J. Cell. Biochem., 56 (1994) 455.
43. Cai, S., Dufner-Beattie, J.L. and Prestwich, G.D., Anal. Biochem., 326 (2004) 33.

Supplementary material

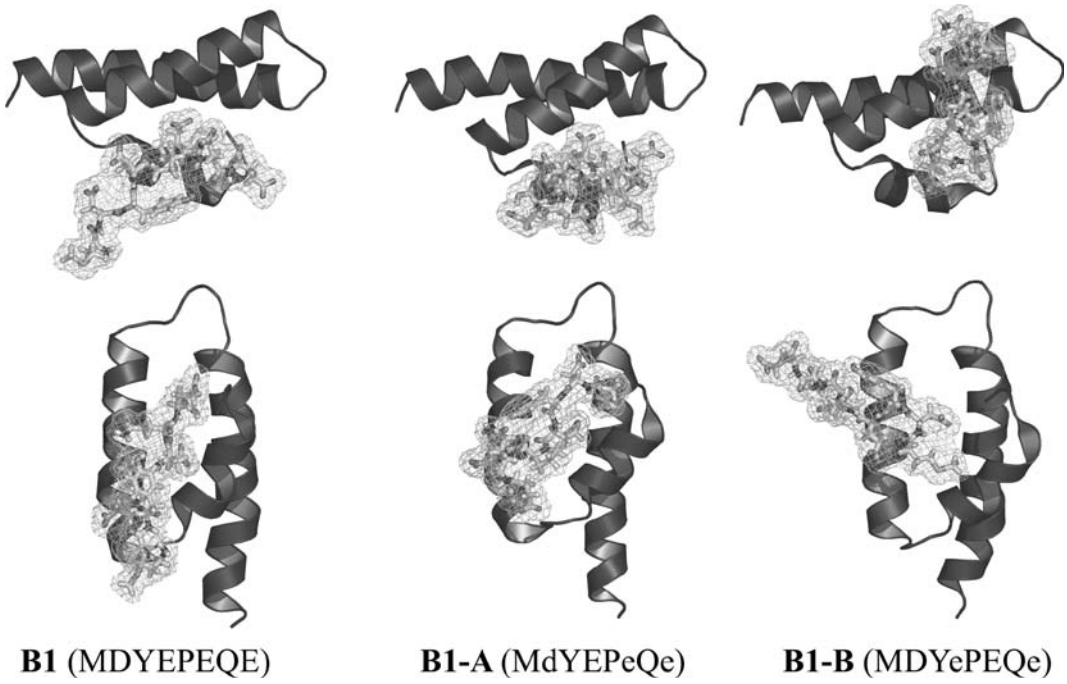

Figure S1. Two views (stacked) of the structures of the B1 series of peptide-ligands docked onto RHAMM(517–576). Within the amino acid sequence of each ligand bound, lower case letters denote D amino acids and upper case letters denote L amino acids.

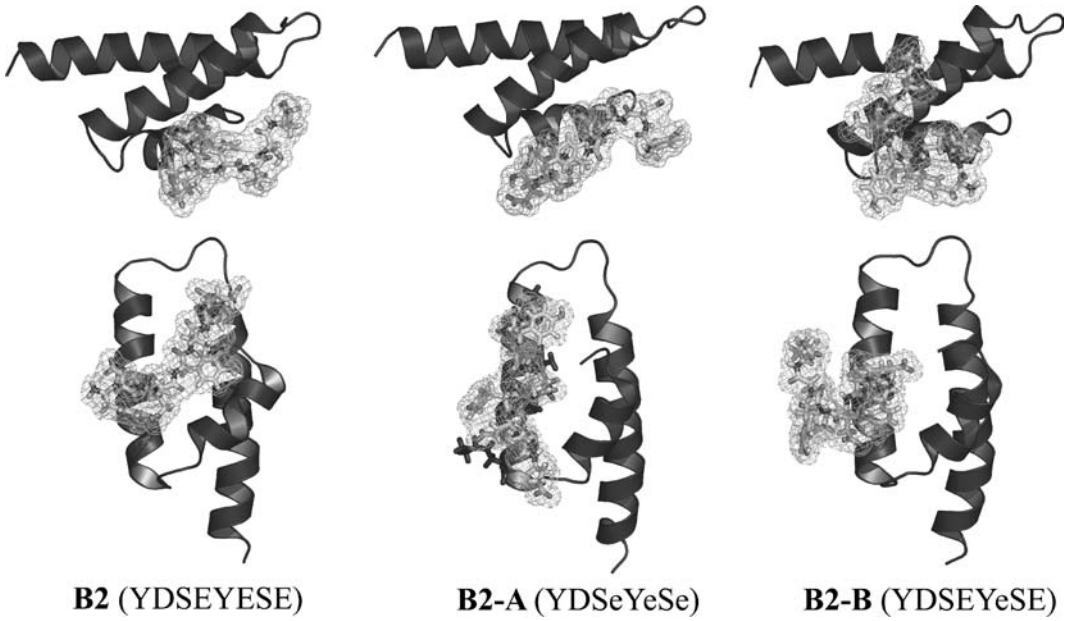

Figure S2. Two views (stacked) of the structures of the B2 series of peptide-ligands docked onto RHAMM(517–576). Within the amino acid sequence of each ligand bound, lower case letters denote D amino acids and upper case letters denote L amino acids.

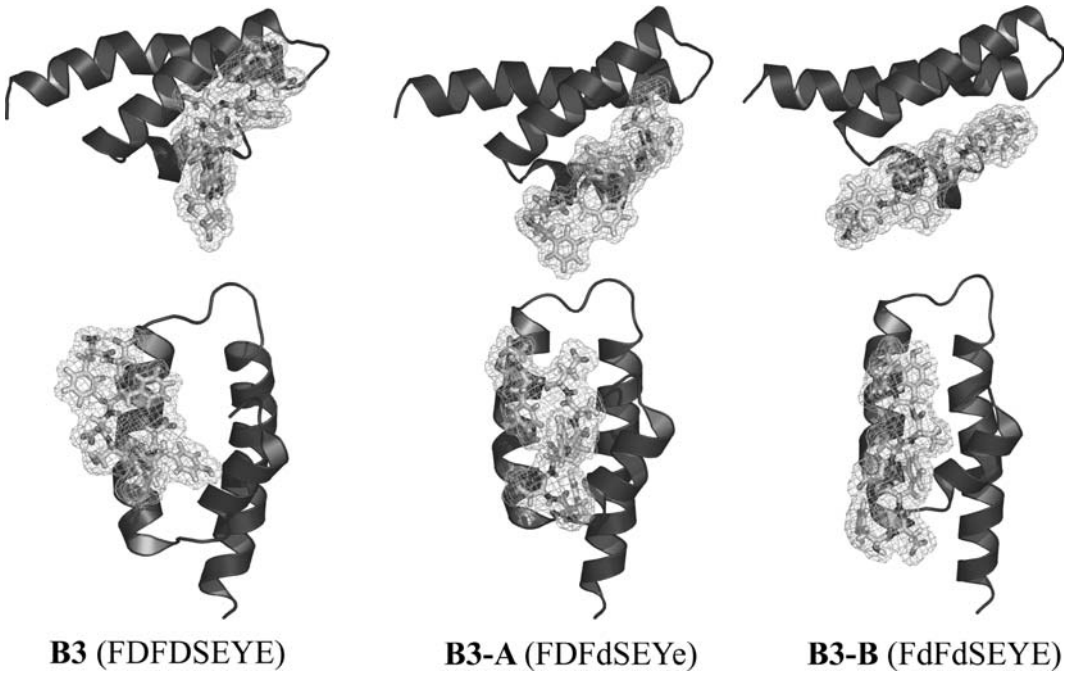

Figure S3. Two views (stacked) of the structures of the B3 series of peptide-ligands docked onto RHAMM(517–576). Within the amino acid sequence of each ligand bound, lower case letters denote D amino acids and upper case letters denote L amino acids.

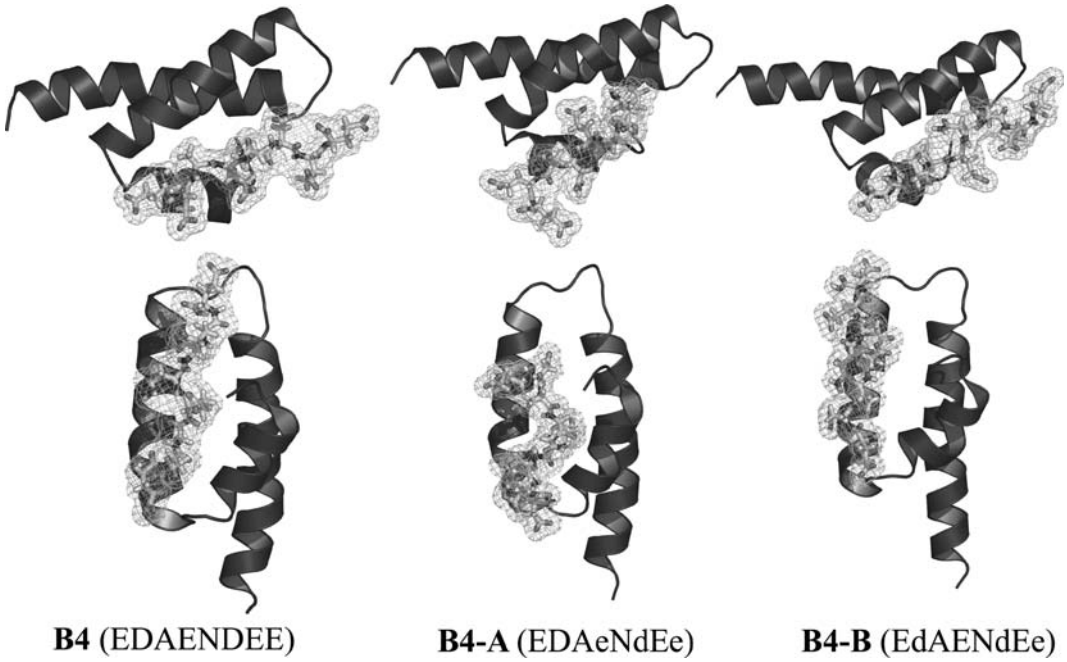

Figure S4. Two views (stacked) of the structures of the B4 series of peptide-ligands docked onto RHAMM(517–576). Within the amino acid sequence of each ligand bound, lower case letters denote D amino acids and upper case letters denote L amino acids.

Table S1. Dock parameters used for all final docking protocols with HA and peptide-ligands on RHAMM(517–576).

DOCK parameter	Value	DOCK parameter	Value
flexible_ligand	no	contact_clash_penalty	50
orient_ligand	yes	chemical_score	yes
score_ligand	yes	energy_score	yes
minimize_ligand	yes	atom_model	u
multiple_ligands	no	vdw_scale	1
random_seed	3	electrostatic_scale	1.7
match_receptor_sites	yes	contact_minimize	yes
random_search	yes	chemical_minimize	yes
ligand_centers	no	energy_minimize	yes
automated_matching	yes	initial_translation	1
maximum_orientations	500	initial_rotation	0.1
write_orientations	no	maximum_iterations	10
rank_orientations	yes	contact_convergence	0.1
rank_orientation_total	100	chemical_convergence	0.1
intermolecular_score	yes	energy_convergence	0.1
gridded_score	yes	maximum_cycles	50
grid_version	4	cycle_convergence	0.1
bump_filter	yes	contact_termination	0.1
bump_maximum	0	chemical_termination	0.1
contact_score	yes	energy_termination	0.1